Thickness effect on the structure and superconductivity of $Nd_{1.2}Ba_{1.8}Cu_3O_z$ epitaxial films

M. Salluzzo,[1] G. M. de Luca,[1,2] D. Marrè,[3] M. Putti,[3] M. Tropeano,[3] U. Scotti di Uccio,[1,4] and R. Vaglio[1]
[1]*COHERENTIA CNR-INFM and Dipartimento di Scienze Fisiche, Università di Napoli "Federico II" Piazzale Tecchio 80, I-80125 Napoli, Italy*
[2]*COHERENTIA CNR-INFM and Dipartimento di Scienze Fisiche, Università di Salerno, Via S. Allende, I-84081 Salerno, Italy*
[3]*LAMIA CNR-INFM and Dipartimento di Scienze Fisiche, Università di Genova, Via Dodecaneso 33, I-16146 Genova, Italy*
[4]*DiMSAT, Università di Cassino, Via di Biasio 43, I-03043 Cassino, Italy*
(Received 28 April 2005; revised manuscript received 26 July 2005; published 25 October 2005)

We have studied the effect of thickness on the structure and superconductivity of $Nd_{1.2}Ba_{1.8}Cu_3O_z$ (NdBCO) epitaxial films deposited on $SrTiO_3$ (100) substrates. High-quality NdBCO films were deposited by high oxygen pressure sputtering. The samples have been carefully characterized by transport measurements and x-ray diffraction using conventional and synchrotron radiation sources. Two structural transformations are observed. The first one is a crossover from the orthorhombic and twinned structure, typical of thick samples, to a pseudotetragonal phase at thickness lower than 60 unit cells. The pseudotetragonal phase exhibits peculiar x-ray diffuse scattering around the Bragg reflections, associated with nanostructured twinned domains. The second one appears at a thickness lower than 20 unit cells and is assigned to a pseudotetragonal-tetragonal transition. The transport properties are not modified at the first crossover, while a substantial decrease in T_c and in the number of holes is observed at the pseudotetragonal-tetragonal transformation. Our results suggest that the structural rearrangement and the transport properties are explained by the ordering of Cu(1)O chains. A simple model, able to explain the experimental results and capturing the essential features of the Cu(1)O chains nucleation process in the $R_{1+x}Ba_{2-x}Cu_3O_{7-\delta}$ (R=Y and rare-earth elements) compounds, is presented.

DOI: 10.1103/PhysRevB.72.134521 PACS number(s): 74.72.−h, 74.62.Dh

I. INTRODUCTION

The microscopic mechanism of high critical temperature superconductivity is still uncertain. Nevertheless, there is a number of theoretical models that predict the effect, on the superconducting and normal state properties, of modifications of key parameters, as the chemical potential μ and the hole density n.[1] In principle, it is possible to tune both μ and n acting on the properties of the charge reservoir and of the CuO_2 layers. Some studies focused on the effects induced by chemical substitution of isovalent ions in the structure (chemical strain),[2] or produced by external hydrostatic pressure.[3] These experiments are difficult to interpret because, due to the complex structures of the high-temperature superconductors (HTS), it is hard to achieve controllable changes in the relevant distances in the CuO_2 planes without any other consequence. Many other efforts have been made to determine and understand the temperature versus hole-doping phase diagram that shows an outstanding generality among the whole HTS family.[4] Unfortunately hole carriers are typically altered by chemical substitution, that inherently introduces disorder and structural modifications in the compounds.

A very convenient way to study the role of hole doping that circumvents such difficulties is carrier injection by electric-field effect. Recently, following this approach, we have modified the hole density in thin $Nd_{1.2}Ba_{1.8}Cu_3O_z$ (NdBCO).[5,6] More precisely, we used thin (NdBCO) films that, due to the Nd-rich composition and strain-related effects, were on the Mott-insulating side of the HTS phase diagram.[6] We demonstrated reversible changes of the resistivity in NdBCO films, and in one case we observed an insulating to superconducting transition. Our results support the idea that hole doping plays a major role in the superconductivity mechanism of the HTS, at least in strongly underdoped samples. Triscone *et al.*[9] modified the critical temperature of stoichiometric 2-unit cells $Nd_1Ba_2Cu_3O_z$ that, however, were characterized by a strongly reduced T_c compared to thick samples. The main problem in this type of experiment is that very thin films must be employed, that may possess physical properties different from the bulk. Indeed, it is well known that the critical temperature of $Re_{1+x}Ba_{2-x}Cu_3O_{7-\delta}$ (RBCO, Re=rare earth or Y) thin films is always depressed irrespective of the kind of strain field to which the structure is subjected,[7] a result that is at odds with the T_c doubling of in-plane compressed $La_{1.9}Sr_{0.1}Cu_2O_6$ films.[8] As a matter of fact in this context, it is very important to investigate the thickness effect on the properties of HTS films. First of all, it is necessary to understand the effect of structural changes and strain in the properties of the HTS films and devices; second, these studies are quite important in order to get a deeper understanding of field effect experiments where very thin films are used.

In this paper, we present a detailed study on the thickness effect on the structure and superconductivity of NdBCO epitaxial films deposited on $SrTiO_3$ (STO) (100) substrates. The choice of this compound for this study is related to a number of interesting features that it exhibits: Nd-rich films (with $x \geqslant 0.1$) show a very good in-plane matching with STO (100) single crystals, very smooth and stable surfaces[10] and, as shown below, $Nd_{1.2}Ba_{1.8}Cu_3O_z$ films grow pseudomorphically and untwinned up to a very large thickness with in-plane parameters matching the STO lattice. Notwithstanding, it shows a superconducting-insulating transition associated with the thickness.[6]

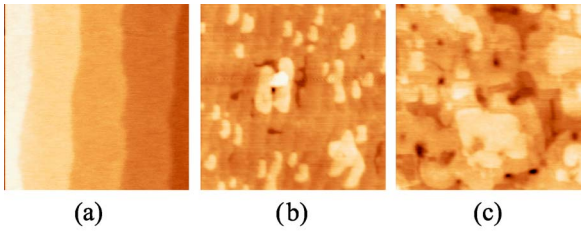

FIG. 1. (Color online) AFM topography obtained in contact mode of (a) an etched and thermal treated $SrTiO_3$ substrate, (b) an 8 u.c., and (c) a 112 u.c. NdBCO film. Each image is 1×1 μm^2 area, while the height scales are (a) 0–2 nm, (b) 0–3 nm, and (c) 0–5 nm.

Section II describes the experimental procedures used to grow and characterize NdBCO samples. In Sec. III, the structural properties as a function of the thickness are presented and analyzed. The transport properties of NdBCO films are shown in Sec. IV, where the temperature dependence of the resistivity and the temperature dependence of the Seebeck effect as a function of the number of unit cells are examined. Finally, the results are discussed and critically analyzed in Sec. V, where we interpret and correlate the structural and the transport properties.

II. DEPOSITION AND CHARACTERIZATION OF NdBCO FILMS

NdBCO films were deposited on 10×10 mm^2 STO (100) single crystals using the high oxygen pressure diode sputtering from a single target at 230 Pa of 95% oxygen and 5% argon as sputtering gas, a target to substrate distance of 15 mm, and a deposition temperature, referred to here as the heater temperature, of 1120 K. Details on the deposition procedure used to get optimized films are presented elsewhere.[11] The STO (100) substrates were etched in order to clean and reconstruct the terrace structure.[12] The procedure consisted of a chemical etching in a BHF solution (pH=5.5) and, just before the deposition, an annealing at 1200 K in pure oxygen. Friction and topography measurements performed in contact mode using an atomic force microscope (AFM), showed well ordered, TiO_2 terminated and slightly vicinal surfaces with a typical terrace width of 200 nm (miscut angle $\alpha\cong0.1°$) [Fig. 1(a)]. As shown in Figs. 1(b) and 1(c), the surface of NdBCO thin films is composed of a two-level terrace structure, with steps typically 0.4 nm high. NdBCO films grow by two-dimensional (2D) nucleations and coalescence of islands resulting in an extremely smooth surface at a thickness above 100 nm. The root-mean-square roughness, measured on a 5×5 μm^2 area, is below 1 nm for 120 nm thick films and 0.4 nm for 10 nm thin films.

Systematic x-ray diffraction measurements were mainly performed by a conventional three-circle Cu $K\alpha$ diffractometer (Rikagu). Some additional data, obtained on 80-, 52-, and 8-unit-cell NdBCO films using synchrotron radiation, will be also presented. The grazing incidence x-ray diffraction (GXID) experiments were carried out at the ID32 surface diffraction and standing waves beamline at the European Synchrotron Radiation Facility (ESRF). More details on the experimental technique can be found in Ref. 13. The very high quality of the structure of these films is clearly confirmed by the full width at half maximum (FWHM) of the rocking curves measured by the conventional diffractometer on symmetric as well as asymmetric reflections: This width is 0.03° on the (001) peak and lower than 0.10° on the (005) and (308) peaks. Reflectivity oscillations, merging with Pendellösung fringes present around the (001) reflection (Fig. 2), are observed for films as thick as 100 nm, demonstrating very smooth surfaces and structural coherence. The number of unit cells can consequently be measured by x-ray diffraction within the precision of 1 unit cell. For convenience, the film thickness will be reported in unit cells (u.c.) in the following. Films with thickness in the range 8–120 u.c. have been investigated.

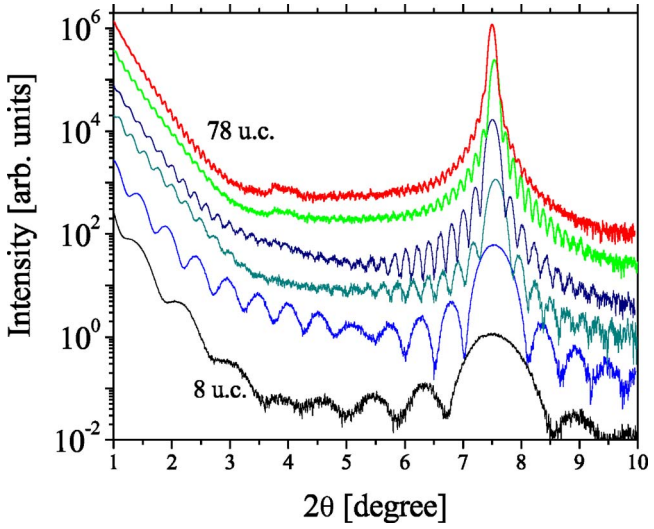

FIG. 2. (Color online) Low angle ϑ-2ϑ diffraction spectra measured on 8, 14, 29, 37, 59, and 78 u.c NdBCO films. Each scan has been displaced by a fixed offset for clarity. Note the reflectivity oscillation merging with Pendellösung fringes around the (001) reflection from which an accurate estimation of film thickness is obtained.

Thick NdBCO films are characterized by a critical temperature (zero-resistivity criteria) of 63–65 K. This value is due the average Nd excess.[14] As a result, these samples are on the underdoped side of the phase diagram, as also confirmed by Seebeck effect measurements (see below).

III. STRUCTURAL PROPERTIES

Systematic measurements of the lattice parameters as a function of the number of unit cells have been performed by conventional x-ray diffraction measurements on symmetric, as well as asymmetric reflections. X-ray diffraction on the (005) peak allowed c-axis length determination. a and b evaluation is instead achieved resorting to ω-2ϑ maps around the (038)-(308) reflections (where ω is the degree of freedom associated with the tilting of the sample around an axis parallel to one of the in-plane lattice parameters, and 2ϑ the Bragg detector angle). The values of a, b, and c have

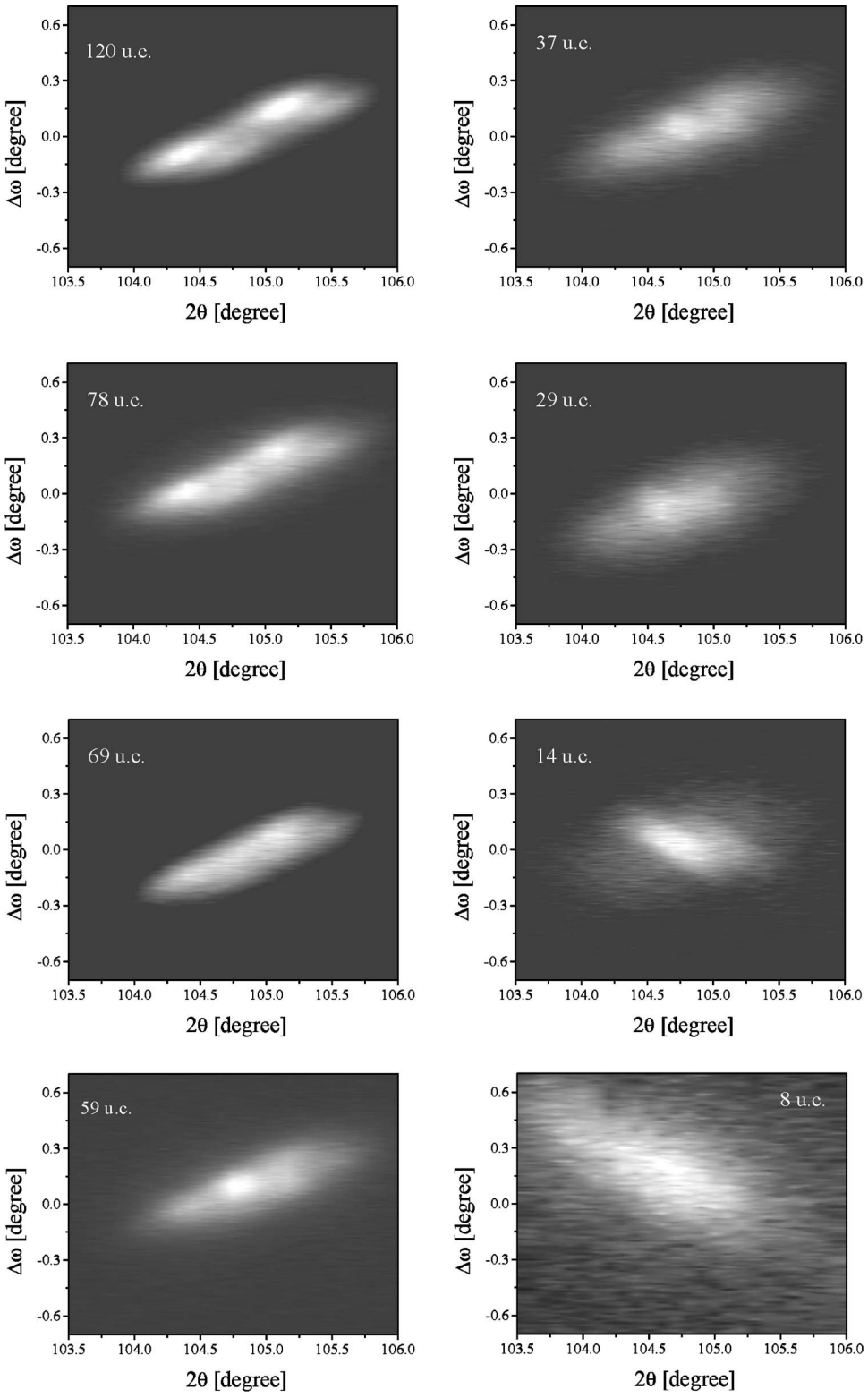

FIG. 3. ω-2ϑ maps around the (0 3 8)-(3 0 8) reflections of Nd-BCO characterized by different thicknesses: 120 u.c., 78 u.c., 69 u.c., and 59 u.c. on the left, and 37 u.c., 29 u.c., 14 u.c., and 8 u.c. on the right. The data have been fitted using a standard 2D-Lorentizian profile (not shown).

been obtained by a fitting procedure, involving a one-dimensional Lorentian profile for (005) peaks, and a 2D Lorentian for the (038)/(308) maps. The experimental errors on the measured lattice parameters are estimated by assuming an uncertainty in the position of the (308)/(038) and of the (005) peaks of 0.03° and 0.004°, respectively. In order to improve the statistics, long acquisition times (up to 2 days) were employed in the case of very thin samples. The (005) peak has been detected before and after long data acquisition, in order to exclude possible oxygen loss during the measurements. In the case of very thin films ($t \leqslant 8$ u.c.), a sensitive variation of the c axis was in some cases detected. For this reason, a few samples were protected by 20 nm amorphous Al_2O_3 deposited *in situ* following the procedure described in

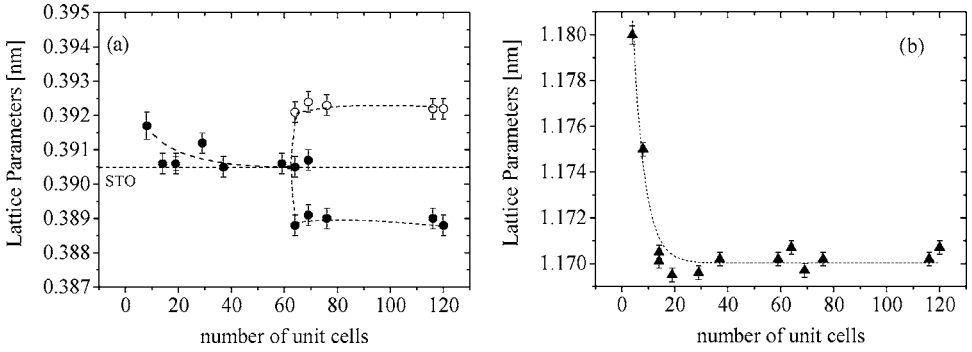

FIG. 4. (a) Measured a (filled circles) and b (open circles) lattice parameters and (b) measured c axis (filled triangles) of the NdBCO films deposited on STO substrates plotted against the number of unit cells. Dashed lines are a guide for the eyes.

Ref. 6. The very low rate and large substrate-film distance (0.04 nm s^{-1} and 13 cm, respectively) suggest that Al_2O_3 deposition should not damage NdBCO. We also verified experimentally that the deposition of the new layer has a negligible effect on the structural and transport properties of films with a thickness larger than 7 u.c.

Thick NdBCO films are orthorhombic and twinned as demonstrated by the presence of two clear peaks in the (308)/(038) maps associated with diffraction from domains with a and b axes, respectively, parallel and perpendicular to the a and b of the STO substrate. The lattice parameters are notably different from the expected values for the $Nd_{1+x}Ba_{2-x}Cu_3O_z$ solid solution (Nd123ss) at $x=0.2$.[15] Both a and b axes are larger than the Nd123ss lattice parameters, while the c axis is shorter. In particular, we have found $c=1.1698\pm0.0003$ nm, $a=0.3892\pm0.0003$ nm, and $b=0.3920\pm0.0003$ nm, instead of $c=1.1715$, $a=0.3870$ nm, and $b=0.3910$ of Nd123ss.[15] The area of the ab rectangle is equal to the area of the in-plane unit cell of STO. These results suggest that 120 u.c. films are still under strain. In order to clarify this question, we have deposited 120 u.c. NdBCO samples on $LaAlO_3$ (100) single crystal characterized by $a=b=0.3780$ nm. Due to the very large mismatch in this case, we expect that thick NdBCO films on $LaAlO_3$ are relaxed. As a result, we found for these films $a=0.3873$ nm, $b=0.3910$ nm, and $c=1.1715$; in very good agreement with the bulk parameters expected for the $x=0.2$ composition from Ref. 15.

However, the lattice parameters of NdBCO can be strongly influenced by the oxygen content, which may explain the differences between our thick films deposited on STO substrates and the Nd123ss. For this reason, we have modified the oxygen content of the 120 u.c. films by using two different procedures.[16] The first one consisted of annealing of a well oxygenated orthorhombic film, in a reducing atmosphere composed of 25 Torr of pure Ar gas at 773 K. The second process consisted of the deposition of a 120 u.c. followed by an annealing procedure, that normally is used to oxygenate the sample, in the reducing atmosphere of Ar gas. In both cases, the overall characteristics of the samples depend only on the annealing time. For relatively short annealing (1 h), the films undergo the orthorhombic to tetragonal transition preserving a T_c of about 37 K. The lattice parameters become $c=1.1720$ nm (slightly longer then the oxygenated samples) and $a=b=0.3904$ nm, identical to the STO substrate lattice parameters within the experimental error. A longer annealing (40 h) leads to the insulating—not oxygenated—phase, with an elongated c-axis (1.1770 nm), but the a and b axes are still equal to the STO substrate. On the basis of Ref. 15, oxygen reduced (quenched) NdBCO (tetragonal, not superconducting samples), are characterized by $a=b=0.3890$ nm.

These experiments indicate that 120 u.c. orthorhombic films deposited on STO are still strained and remain strained when we take out oxygen from the samples.

In Fig. 3 the evolution with thickness of (3 0 8) asymmetric maps is shown, while in Fig. 4 the summary of the results concerning the in-plane and out-of-plane lattice parameters are presented. As shown in Figs. 3 and 4, above 70 u.c., the films remain orthorhombic with nearly constant lattice parameters. At about 70 u.c., we see the appearance of an additional central peak exactly in the middle of the two orthorhombic reflections. Finally, at thickness lower then 60 u.c., the two orthorhombic peaks disappear leaving a central Bragg peak and wings of diffused intensity. It is worth noting that the distance of the side wings from the main reflection, in terms of in-plane scattering vector Δq, is independent of the reflection order, as checked by comparing (2 0 8), (3 0 8), and (4 0 8) maps. Consequently, it is possible to exclude the simultaneous presence in the sample of a main tetragonal phase together with an orthorhombic and twinned phase. Indeed, in that case, the side peaks should correspond to Bragg reflections, whose position scale as a function of reflection order ($h\cdot\Delta q$) should be approximately constant.[17] By rotating the sample along the surface normal by an azimuthal angle of 90°, an identical result is found. The presence of a unique peak indicates that at the macroscopic level the structure is tetragonal. The wings, however, for reasons that will be discussed next, indicate deviations from the tetragonal structure at the nanometer scale. Therefore, below 60 u.c., the NBCO films are pseudotetragonal, i.e., an orthorhombic to pseudotetragonal transition occurs. The lattice parameters of the pseudotetragonal film almost perfectly match the STO lattice down to 14 u.c. At the same time, we can clearly see that the c axis remains almost constant. At about 14 u.c., the elongated diffused intensity typical of the thicker films changes shape. By further decreasing the thickness, we observe an evolution of the (3 0 8) maps and a change of the lattice parameters for the 8 u.c. films for which both the in-plane lattice and c axis are expanded.

In order to better interpret the data, it is useful to work in the reciprocal space. The ω-2ϑ maps around (H 0 L) or (0 K L) reflections are H-L or K-L maps in the reciprocal

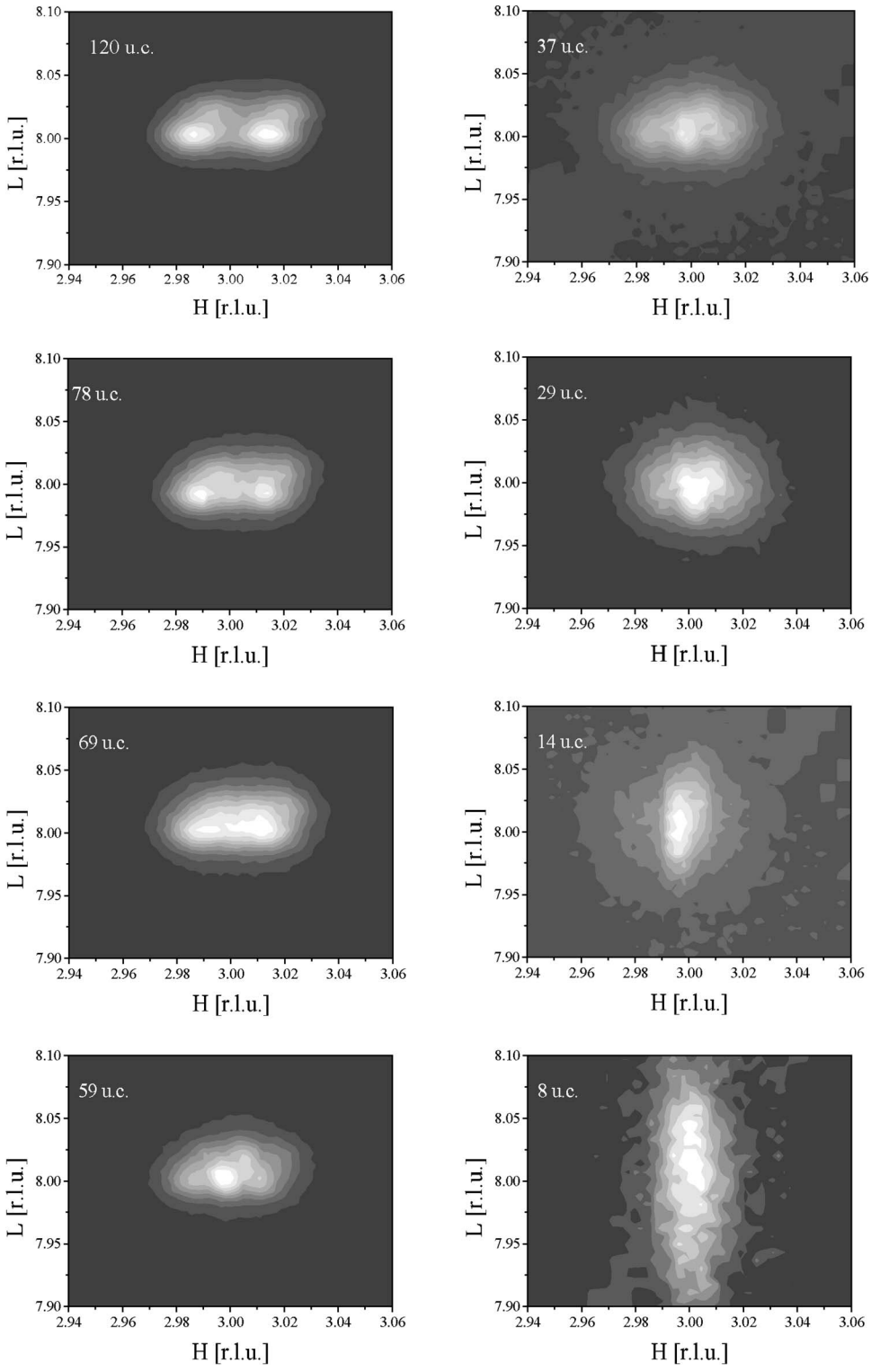

FIG. 5. *H*-*L* (*K*-*L*) maps obtained through coordinate transformation from the ω-2ϑ maps of Fig. 3 measured around the (3 0 8)/(0 3 8) reflections of each sample in function of the thickness: 120 u.c., 78 u.c., 69 u.c., and 59 u.c. on the left and 37 u.c., 29 u.c., 14 u.c., and 8 u.c. on the right.

space. We can reconstruct the *H*-*L* (*K*-*L*) map in a region of the reciprocal space around the (3 0 8) [(0 3 8)] reflection (Fig. 5), by applying a coordinate transformation, taking into account the tetragonal (or orthorhombic) symmetry of the film lattice and by performing a correlation gridding procedure on the data. We see that above 60 u.c., two clear peaks are present on the left and on the right of H (K)=3. The in-plane STO lattice parameters have been used as reciprocal lattice base for convenience. At 60 u.c., only one peak at H =3 is present, but a diffused intensity persists along H. We associate these features with a pseudotetragonal phase. On the contrary, the shape of *H*-*L* maps of 14 u.c. films becomes almost symmetric in L and H. This is related to the decrease of the thickness (that broadens the peak along L due to the finite size effect) and to the disappearing of the diffused features along H indicating the pseudotetragonal to tetragonal transformation. Finally, 8 u.c. films present a shape elongated in the L direction, that is well associated with the size effect.

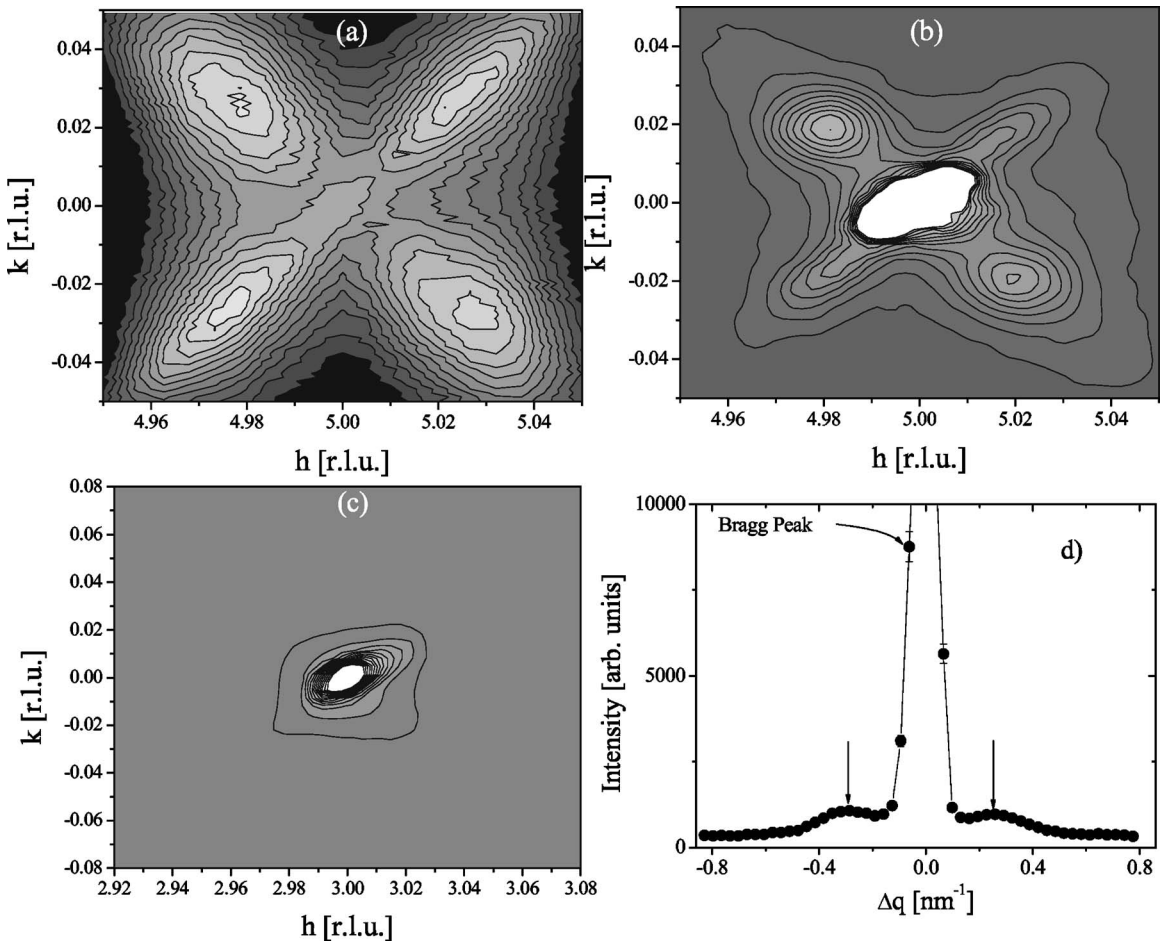

FIG. 6. *H-K* maps obtained through synchrotron radiation GXID on NdBCO samples: (a) (5 0 8) map on 80 u.c. sample; (b) (5 0 8) map on 52 u.c. sample; and (c) (3 0 8) map on 8 u.c. film. (d) Intensity vs in-plane scattering vector along the (110) direction of a 52 u.c. film showing the superstructure features (indicated by arrows) around the main Bragg peak.

The presence of the transitions mentioned above is also clearly visible by comparing (*H-K*) maps performed by GXID using synchrotron radiation on 80, 52, and 8 u.c. samples (Fig. 6). 80 u.c. films are orthorhombic and twinned; therefore, the (5 0 8) map exhibits four peaks almost symmetric around the (5 0 8) reciprocal space position, corresponding to the presence of four different domains, two of which form an angle $2\delta=\tan(\eta)$ between them and the other two obtained by exchanging the respective *a* and *b* axes. Here, $\eta=(b-a)/(b+a)$ is the orthorhombicity coefficient. The (5 0 8) map of a 52 u.c. film is completely different. There is a main peak located exactly at (5 0 8). However, beside the tetragonal peak, four additional weaker structures appear. These features are almost symmetrical around the center. The shape of the satellites is notably different in the (110) and $(1\bar{1}0)$, a result that may be attributed to characteristic features of the growth mode or to the broken symmetry induced by the slight vicinality of the substrate. The position of the satellite peaks remains at constant Δq, with respect to the Bragg peak and irrespective of the reflection order (as demonstrated by maps on other reflections not shown here). Similar features were previously observed on $Sm_1Ba_2Cu_3O_{7-\delta}$[17] and $Gd_1Ba_2Cu_3O_{7-\delta}$[18] thin films deposited on STO (100) substrates and attributed to a tweed structure due to the exchange of oxygen ions among the chain and antichain sites. As demonstrated by previous works made on Al-doped YBCO single crystals,[19] the characteristic shape of the *H-K* maps can be explained by taking into account the contribution of thermal and Huang (static displacement) diffuse scattering associated with disordering of oxygen ions in the chains. Monte Carlo simulations on YBCO (Ref. 20) and Al-doped YBCO (Ref. 21) have shown that a tweed structure, mimicking an ordering of the oxygen ions along the *a* and *b* axes, gives rise to the observed diffracting features. As consequence in the disordered crystals, short chains are formed along both the *a* and *b*, without the formation of twinned domains and with an average tetragonal structure. In NdBCO films, this effect can be associated with the Nd–Ba disorder and to the role of thickness in the stability of long chains, as will be discussed further below. Finally, the (3 0 8) map performed on the 8 u.c. film has a very different shape. A very sharp tetragonal peak is present at the (3 0 8) reciprocal lattice point and the wings characteristic of the 52 u.c. sample disappeared.

Summarizing two structural transformations are observed using asymmetrical reciprocal space maps performed by a conventional x-ray diffraction and by synchrotron radiation. The first one appears at about 70 u.c. and is assigned to a pseudotetragonal (thickness <60 u.c.) to orthorhombic

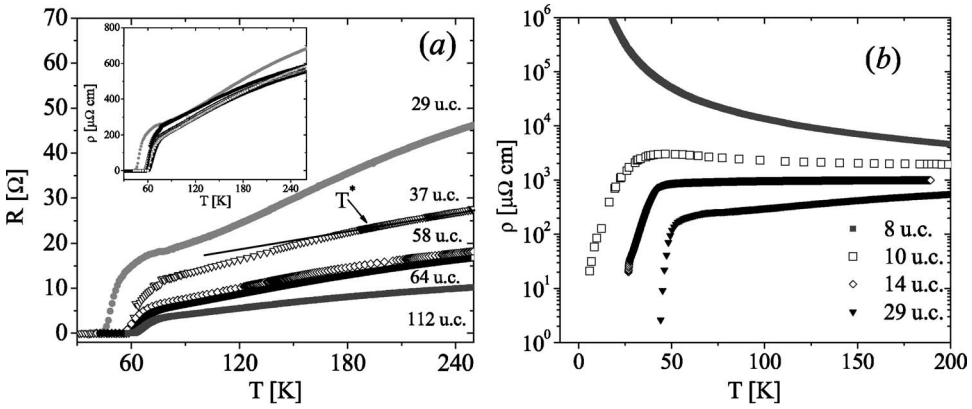

FIG. 7. (a) dc four-probe measurements on NdBCO films with thickness ranging between 120 and 14 u.c. In the inset, the data are reported as resistivity vs temperature; (b) resistivity vs temperature of samples with thicknesses ranging between 20 and 8 u.c.

transformation; the second one corresponds to a pseudotetragonal (thickness < 20 u.c.) to tetragonal transition whose signature is the disappearance of diffuse scattering features around the main Bragg peak.

IV. TRANSPORT PROPERTIES

The thickness dependence of the transport properties have been studied by dc resistivity and Seebeck effect measurements. The resistivity versus temperature data have been collected using a conventional four-probe technique. In Fig. 7(a), the temperature dependence of the resistivity of the 29 to 112 u.c. samples is shown, while the experimental results for films with thickness lower than 29 u.c. are plotted in Fig. 7(b). First of all, we observe that normal state resistivity exhibits a temperature dependence typical of underdoped samples, as shown by the presence of a pronounced curvature in the data below the so-called T^* temperature (approximately indicated by an arrow), usually interpreted as the pseudogap transition temperature. The resistivity of samples with a thickness between 37 to 120 u.c. is remarkably similar, demonstrating that not only the T_c but also the normal state properties, including the curvature at T^*, are not changed by decreasing the thickness across the orthorhombic-pseudotetragonal transition. On the contrary, 29 u.c. and especially 14 u.c. films present a dramatic change in T_c and of the normal state properties. The superconductivity is strongly suppressed in films with thickness lower than 20 u.c. In particular at 8 u.c., a superconducting to insulating transition is observed. As shown in Ref. 6, the temperature dependence of the resistivity of 8 u.c. films is well explained by a variable range hopping mechanism of conduction in the 2D-Mott limit. Therefore, the insulating state is realized because of the localization of the hole carriers.

We performed Seebeck effect experiments on some selected samples in order to gain information about the changes in the number of holes per CuO_2 plane as a function of the thickness. The measurements were performed in a home-built cryostat working from 80 to 300 K. The thermopower was measured by an ac technique, described elsewhere,[22] in a steady flux configuration in which the heat flow is supplied to one end of the sample (cut in pieces of 5×10 mm^2) by a strain-gauge heater (1×1 mm^2), while the other end is in thermal contact with the heat sink. The temperature difference was measured with Au(Fe)-Kp thermocouples, and the electrical contacts to 99.99% Cu wires were made with Ag varnish painted on the Ag contacts previously deposited on the sample. The gradient applied to the sample was varied from 1 to 0.1 K/cm; the frequency was chosen as low as $f=0.005$–0.003 Hz in order to avoid a reduction of the heat wave amplitude along the sample. It is well known that the Seebeck effect in high T_c cuprates is related to the number of holes per CuO_2 plane, p_{pl}, independent from the analyzed compound. In particular, the absolute value of $S(T)$ exhibits a strong systematic decrease with p_{pl}: The room-temperature value S_{290}, that is a convenient parameter, falls nearly exponentially with the number of holes, from 500 μV/K for the underdoped insulating samples ($p_{pl} \cong 0$) to 1–2 μV/K in the case of optimal doping, and reaches the negative value -15 μV/K- at $p_{pl} \cong 0.3$. Many cuprates, despite the different combinations of constituent atoms, stoichiometries, and number of CuO_2 superconducting layers, follow this general trend so closely that a universal correlation between S and p_{pl} was established by Orbetelli *et al.* conveniently parameterized by the relations:[24]

$$S_{290} = 372 \exp(-32.4 \cdot p_{pl}) \text{ for } p_{pl} < 0.05 \quad (1a)$$

$$S_{290} = 992 \exp(-38.1 \cdot p_{pl}) \text{ for } 0.05 < p_{pl} < 0.15 \quad (1b)$$

$$S_{290} = -139 \cdot p_{pl} + 24.2 \text{ for } p_{pl} > 0.155 \quad (1c)$$

Equations (1a)–(1c) were formulated to describe the Seebeck effect of poly-crystals, and the extension to the Seebeck effect of thin films has to be briefly discussed. To correlate the apparent thermoelectric power of ceramic materials with the *ab*-plane Seebeck effect (S_{ab}), it is necessary to average the contribution of anisotropic grain randomly oriented (without considering the local variation of temperature gradient). As a first approximation, due to the very high anisotropy of underdoped cuprates, the contribution of S_{ab} prevails. Also, taking into account the exponential dependence of the Seebeck effect on p_{pl}, the geometrical correction, that would lead to a maximum correction of 3/2 in the case of thin films having isotropic conductivities,[23] is consequently negligible.

Seebeck effect measurements were performed on thin films with thickness of 8, 14, 29, and 112 u.c. We concentrated on thin films characterized by notable differences in

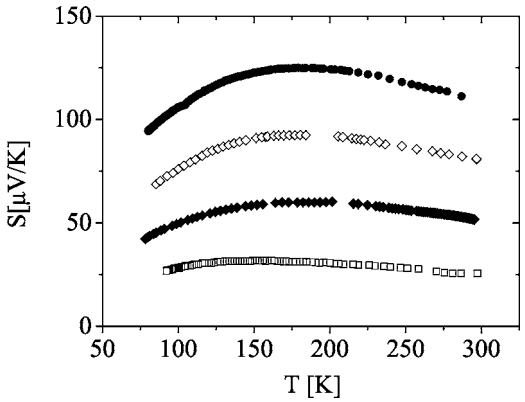

FIG. 8. The measured temperature dependence of the Seebeck effect coefficient for samples characterized by 8 u.c. (filled circles), 14 u.c. (open diamonds), 29 u.c. (filled diamonds), and 112 u.c. (open squares).

resistivity and critical temperatures, while the results obtained on the thick films are used as a reference value. The S versus T plots in the range from 80 to 300 K are reported in Fig. 8. All curves show a similar behavior with a broad maximum around 150–200 K. The absolute value of the Seebeck effect increases as the film thickness decreases: The Seebeck effect at room temperature for the 112 u.c. film is around 30 μV/K, and it increases up to 120–160 μV/K for the 8 u.c. film. This suggests that by decreasing the film thickness the number of holes per CuO_2 planes progressively diminishes.

In Table I, we report S_{290} and p_{pl} values. For the 112, 29, and 14 u.c. films that presented a metallic resistivity and transitions to the superconducting state, we estimated p_{pl} by Eq. (1b). For the 8 u.c films which showed an increasing resistivity with decreasing temperature and any resistive transition to the superconducting state down to 4.2 K, the application of Eq. (1) is less straightforward. Indeed by using Eq. (1b), we obtain a value of 0.054–0.057 on the two 8 u.c. samples investigated, that is near the 0.05 limit. Below this value, Eq. (1a) is instead more appropriate. Since these samples are at the boundary between the superconducting and the insulating state, we prefer to report, in Table I, the average of the values calculated using Eqs. (1a) and (1b). The discrepancy is related to the phenomenological nature of Eq. (1) whose validity has been checked in the middle of the definition range and not at the boundaries. So we can assume an average value of $p_{pl}=0.045$. The hole number per CuO_2 plane shows the following trend: For the 112 u.c. films, p_{pl} is 0.097, on the underdoped side of phase diagram. Then, at decreasing thickness, p_{pl} diminishes down to 0.065 for the 14 u.c. film. For the 8 u.c. film, p_{pl} is about 0.045, that is in agreement with the Mott-insulating behavior of the resistivity.

V. DISCUSSION

As demonstrated in the previous sections, NdBCO films, deposited on STO (100) substrate, exhibit a quite interesting evolution of the structural and transport properties as a function of film thickness. The results can be summarized as follows: (a) Thick NdBCO films are orthorhombic and twinned; (b) below 70 u.c., they are pseudotetragonal with an in-plane lattice identical to the STO lattice and unaltered c axis. The transport properties are not modified with respect to the orthorhombic samples; (c) by further decreasing the thickness, the diffused intensity features—characteristic of the pseudotetragonal phase—disappear at a thickness lower than 20 u.c., while the lattice parameters remain constant down to 14 u.c. pointing to a pseudotetragonal-tetragonal transformation; (d) films with a thickness lower than 10 u.c., on the contrary, exhibit both a clear increase in the lattice (especially a c-axis expansion) and the disappearance of the diffused intensity features characteristic of the pseudotetragonal phase; and (e) both T_c and number of holes decrease in films thinner than 30 u.c., and the very thin films are insulating.

In the next subsections, we analyze the details of these experimental findings and try to rationalize the results in the

TABLE I. Seebeck effect coefficients, calculated number of holes per CuO_2 planes p_{pl}, experimental T_c, and expected critical temperatures following Eq. (2) (Model 1) and Eq. (3) (Model 2) of NdBCO samples with different thicknesses.

Number of unit cells	S(290 K)(μV/K)	p_{pl}	$T_c(R=0)$ (K)	T_c Model 2 (K)	T_c Model 1 (K)
4			0		
8	128	0.045	0	66.1	0
8	111	0.045	0	66.1	0
14	82	0.065	24.0	66.2	24.1
29	52	0.077	43.0	66.2	40.9
37			56.0	66.2	
59			58.0	66.2	
64			60.3	66.2	
69			60.5	64.3	
76			62.0	66.2	
116	25	0.097	64.0	64.3	63.8
120			64.0	66.2	

framework of a possible physical scenario for thin NdBCO films.

A. Superconductivity, strain, and hole doping

We can start our analysis by considering the effect of strain on T_c associated with the application of an equivalent uniaxial pressure:

$$\Delta T_c(\varepsilon_a,\varepsilon_b,\varepsilon_c) = \frac{\partial T_c}{\partial \varepsilon_a}\Delta\varepsilon_a + \frac{\partial T_c}{\partial \varepsilon_b}\Delta\varepsilon_b + \frac{\partial T_c}{\partial \varepsilon_c}\Delta\varepsilon_c, \qquad (2)$$

Here, we can assume that the values of the uniaxial strain $\Delta\varepsilon_i=(a_i-a_{i0})/a_{i0}$ are determined by the change of the lattice parameter with respect to the lattice parameters of a bulk NdBCO ($a_{10}=0.3870$ nm, $a_{20}=0.3910$ nm, $a_{30}=1.1710$ nm).[15] The first difficulty here is that, to our knowledge, experimental data on the uniaxial pressure effect coefficients, $\partial T_c/\partial\varepsilon_i$, of the NdBCO compound are not available. As a first approximation, we can use the values of YBCO.[25] The effect of the pressure on the T_c of RBCO bulk samples has been found to have a remarkable regular trend with the ionic radii at the rare-earth site, with an increase by increasing the R atomic number.[26] Thus, there is no special reason to suppose that the sign of the uniaxial pressure coefficients is different in $Y_1Ba_2Cu_3O_{7-\delta}$ (YBCO) with respect to the other RBCO compounds. These considerations, besides the fact that NdBCO films are underdoped,[27] have the consequence that the absolute value of the calculated T_c shift due to the elastic stress represents a lower bound of the expected value in the case of equivalent uniaxial pressure effect. However, the sign and the general trend should not be modified by the values used in the calculation. As shown in Table I, the elastic stress model foresees a tiny increase in T_c at the orthorhombic to tetragonal transformation and a slight tendency for a T_c increase in the thinnest films. Larger uniaxial temperature coefficients and a change of their sign, in order to match the observed trend, are required to reproduce the experimental results. One of the main reasons is that, at a thickness lower than 60 u.c., the NdBCO lattice is practically unchanged, excepted for the thinnest 8 u.c. films. However, in this case, since the c axis increases, following the model, the T_c is expected to increase even more.

Another very important observation is that the number of holes decreases by decreasing the thickness, and this seems to be correlated with the T_c changes. Consequently, as a second attempt, we tried to calculate the expected critical temperature of NdBCO films using the available data on the number of holes per CuO_2 plane and the phenomenological formula valid for all cuprates:

$$T_c = T_{c\,\max}\cdot\left[1-\left(\frac{p_{\rm pl}-p_{\rm opt}}{\Delta p}\right)^2\right], \qquad (3)$$

where $T_{c\,\max}=95$ K is the maximum T_c of the NdBCO compound, $p_{\rm opt}$ is the optimal doping concentration, and Δp is the half-range of doping for which the compound is superconducting. As shown in Table I, a satisfactory agreement between the experimental and the calculated T_c is obtained for $p_{\rm opt}=0.16$ and $\Delta p=0.11$. Note that with these parameters,

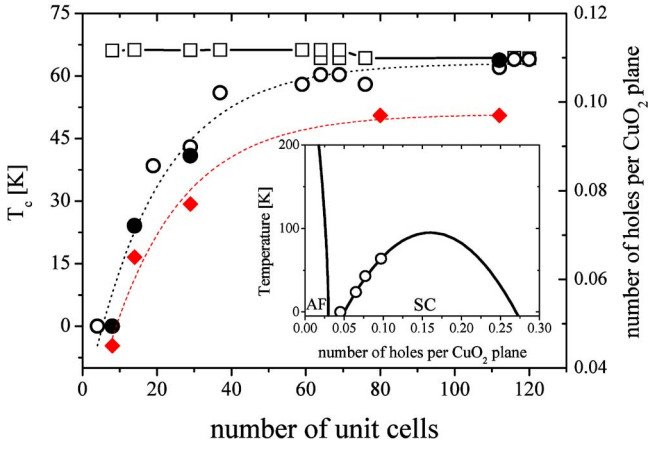

FIG. 9. (Color online) The experimental T_c (zero resistivity criteria) (open circles) and the calculated value of T_c using Eqs. (2) (open squares) and (3) (closed circles), together with the unit cell dependence of the number of holes per CuO_2 plane determined from the Seebeck effect coefficient (closed diamonds).

Eq. (3) reduces to the well-known phenomenological formula $T_c/T_{c\,\max}=1-82.6(p_{\rm pl}-0.16)^2$. In Fig. 9, the experimental T_c and values obtained from both Eqs. (2) and (3) are plotted together with the thickness dependence of the number of holes per CuO_2 plane. It is evident that the T_c dependence with thickness is well correlated with a doping change, while it is not with the uniaxial strain effect. Therefore, it is important to understand why holes decrease with thickness. It is well known that the charge-transfer mechanism in the RBCO family is governed by the transfer of holes from the Cu(1)–O planes, containing O–Cu(1)–O chains, and the CuO_2 planes. Depending on the oxygen content and on the disorder, the number of holes may change. When the compounds have an oxygen content lower than a given value, dependent on the rare earth, superconductivity disappears. At the same time, the structure becomes tetragonal due to the disordering of oxygen among the chain and the antichain sites. This effect is favored by the presence of Nd excess in the NdBCO films. In thick films ($t>70$ u.c.), oxygen preferentially locates along the b axis, and chains are formed, explaining the orthorhombic and twinned phase. Across the orthorhombic-tetragonal transformation the transport properties of NdBCO films are not changed, suggesting that O–Cu(1)–O chains are still present, but alternatively align in both a and b directions, with a correlation length shorter than the x-ray coherence length, stabilizing an overall tetragonal phase. In this case, the oxygen ions are located alternatively along (1 0 0) and (0 1 0), and the lattice is modulated with a period that is between 8 and 10 lattice constants, as suggested by the position along the (110) direction of the side wings in the H-K map of Fig. 6(d). [The distance between the side wings along the (110) direction is about $\Delta H=0.018$ r.l.u. corresponding to $\Delta q=2\pi/a\cdot\Delta H\cong 0.03$ Å^{-1} and a modulation period of 3.3 nm.] This period also roughly corresponds to the average chain length present in the a and b direction.

The strong suppression of T_c occurs across the pseudotetragonal to tetragonal transformation. On the contrary, no

changes are detected at the orthorhombic to pseudotetragonal transformation. Jiang *et al.*[19] argued that T_c can be suppressed when the chain length becomes comparable with the in-plane superconducting coherence length. Consequently, in the pseudotetragonal phase and from the point of view of superconductivity, the samples are locally orthorhombic since the modulated structure has a period larger than the superconducting coherence length (about 2 nm in this material). This explains why the critical temperature is not modified at the orthorhombic-pseudotetragonal transition. On the contrary, at the pseudotetragonal-tetragonal transition, the chain structure is substantially destroyed leading to a T_c reduction and the end to the superconducting-insulating transition.

The critical analysis of our data allows us to exclude some tentative explanations of the T_c versus t dependence: (1) A role of dimensional crossover is quite unlikely, since the thickness at which the change in the electronic and structural properties of the NdBCO films occurs is quite large; (2) a change in the cationic disorder is also quite unlikely because these would strongly affect the c axis of the film (by decreasing it) that is exactly the opposite of our observation; and (3) the elastic strain and classical relaxation mechanism do not explain either the superconductivity or the structural properties of our films.

We arrived at similar conclusions by studying the mechanism of strain relaxation in Nd-doped YBCO (YNdBCO) films deposited on $LaAlO_3$ substrates. In that case we observed a crossover from orthorhombic to tetragonal structure, below 10 u.c., with lattice parameters very far from the $LaAlO_3$ substrate, together with a decrease in the critical temperature. As in the case of the present results, the thickness dependence of the structure and of the T_c could not be explained in terms of elastic strain of the films, but instead could be ascribed to inelastic deformation associated with the disordering of chains.[28]

B. Thickness effect and structural crossovers

Now we analyze structural transformations observed by decreasing the film thickness. It would be tempting to attribute them to the effect of strain relaxation, that is classically realized at the so-called critical thickness. The critical thickness is determined by the minimization of the interface energy, that, in the case of the edge dislocation mechanism of strain relief, leads to the well-known equation:[29]

$$\frac{\partial e}{\partial \varepsilon_k} t_c = \frac{G b_k}{2\pi(1-\nu)} \left(1 + \ln \frac{t_c}{b_k}\right), \tag{4}$$

where $e = 1/2 \cdot \Sigma_{i,j} C_{ij} \varepsilon_i \varepsilon_j$ is the strain energy, G is the Young modulus, ν is the Poisson coefficient and b_k is the Burgers vector. The anisotropic form of the Ball–van Der Merwe–Matthews model has been applied for the calculation of the energy to create an edge dislocation.[30] Using the C_{ij} coefficients of YBCO (Ref. 31), we get a value of $t_c = 27$ nm that is much lower than 70 nm, the thickness at which the orthorhombic to tetragonal transition occurs and slightly larger than the value at which the pseudotetragonal to tetragonal transition was observed. (The elastic constants among the REBCO family theoretically are similar to one another. Therefore, the error made using the YBCO coefficients is largely compensated for by the experimental uncertainties with which these coefficients are estimated.) It is possible that the formation of the modulated tweed structure at 20 u.c. and of twin domains at 70 u.c. can partially release the strain. However, the relaxation appears to be incomplete even in the very thick films. The main proof of this is the effect of gradual oxygen reduction that leads to films with a different c axis and different transport properties, but an in-plane axis equal to the STO substrate. On the contrary, well-oxygenated films are twinned and orthorhombic, but exhibit lattice parameters notably different from the expected values for the $x = 0.2$ composition.[15] It is remarkable that the in-plane area of the unit cell is exactly that of the STO substrate. It is clear that in the case of our films, Eq. (4) may not apply to our case, because other mechanisms, besides edge dislocations formation, may be relevant.

We propose in the following an alternative explanation of the observed structural transitions, based on the idea that the variation of the oxygen content and ordering strongly affect the RBCO structure.

It is well known that at the deposition conditions, RBCO films have a tetragonal oxygen-deficient structure. In order to obtain a fully oxygenated sample, as in our case, the cooling is accomplished by a high oxygen pressure annealing step at intermediate temperatures (773 K, in our case). During this phase, the oxygen ions are incorporated in the Cu(1)–O planes. There, the nucleation of the chains structure takes place, that is short O–Cu(1)–O chains form and successively grow. At given thermodynamic conditions, a statistical distribution of stable and unstable chains of average length L is present in the film.

The Gibbs free energy G of a small domain with one orientation of the chains can be estimated on simple considerations. There are three main contributions. The first one is the oxygen condensation energy, proportional to the volume of the domain, that is $L^2 \cdot t$, t being the film thickness. Such a term includes two competing contributions: The supersaturation $\Delta\mu$ which depends on the oxygen partial pressure and on the temperature that favors oxygen allocation; and the strain energy which is accumulated in the orthorhombic structure because of the biaxial stress due to substrate. There is then a positive surface energy term, that includes both the presence of the interface with the substrate and with the vacuum. Finally, another positive term comes from the presence of the domain walls (twin boundary), with an area of the order of $L \cdot t$. The total Gibbs energy is then

$$G = -g_{\text{bulk}} \cdot L^2 \cdot t + g_{\text{surface}} \cdot L^2 + g_{\text{twin boundary}} \cdot L \cdot t, \tag{5}$$

where g_{bulk}, g_{surface}, $g_{\text{twin boundary}}$ are the bulk condensation energy per unit volume, the surface energy per unit area, and twin boundary energy per unit area, respectively. Minimization of the Gibbs free energy with respect to L determines the critical size of a domain (the size over which the domain is stable):

$$L^* = \frac{[g_{\text{twin boundary}}/g_{\text{surface}}] \cdot t}{2 \cdot (g_{\text{bulk}}/g_{\text{surface}} \cdot t - 1)}. \tag{6}$$

The first result of the model is that chains are unstable below $t_c = g_{\text{surface}}/g_{\text{bulk}}$. In the case of our experiment, this limit is at $t_c = 8$ u.c. In this regime, it is no more advantageous to form even short O–Cu(1)–O chains. Moreover, in very thin films, the weight of the surface part of the film is very important for the overall stability of the structure. The microscopic analysis of the surface term is quite challenging, because it requires a complete refinement of the structure of NdBCO films as thin as 8 u.c. However, we have strong indications from preliminary GXID experiments at the synchrotron that thin films are characterized by an expanded surface involving at least 3 or 4 u.c. These may explain the strong *c*-axis expansion and the poor superconducting properties. In our opinion, the large differences between thin and thick films are therefore ascribed to the different abilities to incorporate oxygen in the surface structure and in the bulk. The dependence of g_{bulk} on the supersaturation also implies that the structure of very thin films is influenced by the environment conditions during annealing. Moreover, it is reasonable that g_{bulk} and g_{surface} may be sensitive to the initial growth mode and to the microstructures that are formed, consistent with recent studies on YBCO thin films deposited by pulsed laser deposition.[32] A systematic study in function of the deposition conditions and substrate surface termination on the structure and superconductivity of very thin NdBCO films is in progress in order to understand these phenomena.

When the film thickness is increased, chain formation is allowed. However, in order to realize a stable orthorhombic domain, it is necessary to overcome the nucleation energy barrier, given by

$$G^* = \frac{(g_{\text{twin boundary}} \cdot t)^2}{2(g_{\text{bulk}} \cdot t - g_{\text{surface}})}. \tag{7}$$

Such a barrier is higher at a low thickness near $t = t_c$, leading to an exponentially increasing time for the formation of stable, long chains. Therefore, also depending on the environment conditions through the supersaturation $\Delta\mu$, only small domains (i.e., thermodynamic fluctuations) are possible at a low thickness, and are in fact observed in the range of 20–70 u.c. The pseudotetragonal phase is indeed composed of short chains, that keep a short-range order in the film. The pseudotetragonal structure, as already mentioned, keeps some average degree of long-range order, because the lattice is modulated with a fixed length =3 nm. Of course, this effect is not accounted for by the thermodynamical description.

VI. CONCLUSIONS

In conclusion, we have studied the thickness effect on the superconductivity and structure of NdBCO epitaxial films deposited on $SrTiO_3$ (100) substrates. We have shown that NdBCO films deposited by high-pressure oxygen sputtering exhibit two structural transformations: A tetragonal (thickness: 20 u.c.) to a pseudotetragonal structure showing diffuse scattering features around the Bragg peak that we interpret as short-range precursor of the twinned orthorhombic phase; the second phase transition is a pseudotetragonal to orthorhombic twinned phase. It is found that T_c decreases substantially in films with a thickness lower than 20 u.c., well correlated with the decrease in the number of holes per CuO_2, while no change is observed at the orthorhombic-pseudotetragonal transition. Our results suggest that the hole transfer mechanism is the same in the pseudotetragonal and orthorhombic phases, where O–Cu(1)–O chains are formed. On the contrary, superconductivity is depressed and finally disappears in the thinnest samples. Such films are tetragonal and strongly oxygen disordered. The strong reduction in the holes in the Cu(1)–O plane, that is the charge reservoir, finally affects the hole carriers in the conducting CuO_2 planes that—due to the small thickness—are not able to form chain structures involving a number of unit cells lower than the superconducting coherence length, and leading at the end to a Mott-insulating behavior observed in the 8 u.c. films.

ACKNOWLEDGMENTS

The authors are grateful to J. Zegenhagen and F. Miletto Granozio for the useful discussions and suggestions on data interpretation. The help of X. Torrelles and C. Aruta was invaluable during the experiments at the ESRF. The collaboration with I. Maggio-Aprile and E. Koller has stimulated the present work. The staff of the ID32 beamline at the ESRF is gratefully acknowledged for the technical help during the experiments and for sample preparation.

[1] S.-C. Zhang, J.-P. Hu, E. Arrigoni, W. Hanke, and A. Auerbach, Phys. Rev. B **60**, 13070 (1999).

[2] X. J. Chen, C. D. Gong, and Y. B. Yu, Phys. Rev. B **61**, 3691 (2000).

[3] H. Takahashi and N. Mori, in *Studies of High-Temperature Superconductors*, edited by A. V. Narlikar (Nova Science, New York, 1996), Vol. 16.

[4] J. B. Torrance, Y. Tokura, A. I. Nazzal, A. Bezinge, T. C. Huang, and S. S. P. Parkin, Phys. Rev. Lett. **61**, 1127 (1988); Y. Ando, Y. Hanaki, S. Ono, T. Murayama, K. Segawa, N. Miyamoto, and S. Komiya, Phys. Rev. B **61**, R14956 (2000).

[5] A. Cassinese, G. M. DeLuca, A. Prigiobbo, M. Salluzzo, and R. Vaglio, Appl. Phys. Lett. **84**, 3933 (2004).

[6] M. Salluzzo, A. Cassinese, G. M. De Luca, A. Gambardella, A. Prigiobbo, and R. Vaglio, Phys. Rev. B **70**, 214528 (2004).

[7] H. Y. Zhai and W. K. Chu, Appl. Phys. Lett. **76**, 3469 (2000).

[8] H. Sato and M. Naito, Physica C **274**, 221 (1997); J. P. Locquet, J. Perret, J. Fompeyrine, E. Machler, J. W. Seo, and G. V. Tendeloo, Nature (London) **394**, 453 (1998).

[9] D. Matthey, S. Gariglio, and J. M. Triscone, Appl. Phys. Lett. **83**, 3758 (2003).

[10] M. Salluzzo, C. Aruta, I. Maggio-Aprile, Ø. Fischer, J. Zegen-

hagen, and S. Bals, Phys. Status Solidi A **186**, 339 (2001).
[11] G. M. De Luca, G. Ausanio, M. Salluzzo, and R. Vaglio, *Proceedings of the 6th European Applied Conference on Superconductivity*, Sorrento, Italy (2003).
[12] M. Kawasaki, K. Takahashi, T. Maeda, R. Tsuchiya, M. Shinohara, O. Ishiyama, T. Yonezawa, M. Yoshimoto, and H. Koinuma, Science **226**, 1540 (1994).
[13] X. Torrelles, C. Aruta, A. Fragneto, I. Maggio-Aprile, L. Ortega, F. Ricci, J. Rius, M. Salluzzo, and U. Scotti di Uccio, Phys. Rev. B **70**, 104519 (2004).
[14] M. Salluzzo, A. Andreone, F. Palomba, G. Pica, R. Vaglio, I. Maggio-Aprile, and Ø. Fischer, Eur. Phys. J. B **24**, 177 (2001).
[15] E. Goodilin, A. Oka, J. G. Wen, Y. Shiohara, M. Kambara, and T. Umeda, Physica C **299**, 279 (1998); E. Goodilin, M. Limonov, A. Panfilov, N. Khasanova, A. Oka, S. Tajima, and Y. Shiohara, *ibid.* **300**, 250 (1998). See Fig. 3 in the above manuscripts.
[16] See EPAPS Document No. E-PRBMDO-72-085537 for the experimental details and the related data. This document can be reached via a direct link in the online article's HTML reference section or via the EPAPS home page (http://www.aip.org/pubservs/epaps.html).
[17] Q. D. Jiang, D. -M. Smilgies, R. Feidenhans, M. Cardona, and J. Zegenhagen, Solid State Commun. **98**, 157 (1996).
[18] L. X. Cao, T. L. Lee, F. Renner, Y. X. Su, R. L. Johnson, and J. Zegenhagen, Phys. Rev. B **65**, 113402 (2002).
[19] X. Jiang, P. Wochner, S. C. Moss, and P. Zschack, Phys. Rev. Lett. **67**, 2167 (1991).
[20] M. Goldman, C. P. Burmester, L. T. Wille, and R. Gronsky, Phys. Rev. B **52**, 1331 (1995).
[21] Z. -X. Cai, Y. Zhu, and D. O. Welch, Phys. Rev. B **46**, 11014 (1992).
[22] M. Putti, M. R. Cimberle, A. Canesi, C. Foglia, and A. S. Siri, Phys. Rev. B **58**, 12344 (1998).
[23] M. Putti, D. Marrè, I. Pallecchi, P. G. Medaglia, A. Tebano, and G. Balestrino, Phys. Rev. B **69**, 134511 (2004).
[24] S. D. Obertelli, J. R Cooper, and J. L. Tallon, Phys. Rev. B **46**, 14928 (1992); J. L. Tallon, J. R. Cooper, P. S. I. P. N. de Silva, G. V. M. Williams, and J. W. Loram, Phys. Rev. Lett. **75**, 4114 (1995); C. Bernhard and J. L. Tallon, Phys. Rev. B **54**, 10201 (1996).
[25] U. Welp, M. Grimsditch, S. Fleshler, W. Nessler, J. Downey, G. W. Crabtree, and J. Guimpel, Phys. Rev. Lett. **69**, 2130 (1992).
[26] J. G. Lin, C. Y. Huang, Y. Y. Xue, C. W. Chu, X. W. Cao, and J. C. Ho, Phys. Rev. B **51**, R12900 (1995).
[27] C. C. Almasan, S. H. Han, B. W. Lee, L. M. Paulius, M. B. Maple, B. W. Veal, J. W. Downey, A. P. Paulikas, Z. Fisk, and J. E. Schirber, Phys. Rev. Lett. **69**, 680 (1992).
[28] M. Salluzzo, C. Aruta, G. Ausanio, A. D'Agostino, and U. Scotti di Uccio, Phys. Rev. B **66**, 184518 (2002).
[29] J. W. Matthews and A. E. Blakeslee, J. Cryst. Growth **27**, 118 (1974); **32**, 265 (1976).
[30] J. H. van der Merwe and C. A. B. Ball, in *Epitaxial Growth*, edited by J. W. Matthews (Academic, NewYork, 1975), Part B, pp. 493–528; J. W. Matthews, *ibid.*559–609.
[31] M. Lei, J. L. Sarrao, W. M. Visscher, T. M. Bell, J. D. Thompson, A. Migliori, U. W. Welp, and B. W. Veal, Phys. Rev. B **47**, 6154 (1993).
[32] G. Rijnders, S. Curras, M. Huijben, D. H. A. Blank, and H. Rogalla, Appl. Phys. Lett. **84**, 1150 (2004).